Journal of Power Sources 247 (2014) 412–422

Contents lists available at ScienceDirect

Journal of Power Sources

journal homepage: www.elsevier.com/locate/jpowsour

Capacity fade of $LiNi_{(1-x-y)}Co_xAl_yO_2$ cathode for lithium-ion batteries during accelerated calendar and cycle life test. I. Comparison analysis between $LiNi_{(1-x-y)}Co_xAl_yO_2$ and $LiCoO_2$ cathodes in cylindrical lithium-ion cells during long term storage test

Shoichiro Watanabe*, Masahiro Kinoshita, Kensuke Nakura

Portable Rechargeable Battery Business Division, SANYO Electric Co., Ltd, Automotive & Industrial Systems Company of Panasonic Group, 139-32, Toyohisa, Matsushige-Cho, Itano-gun, Tokushima 771-0213, Japan

HIGHLIGHTS

- We investigate the degradation of Li-ion battery during long-term storage test.
- The degradation of Ni based cathode is compared with that of Co based cathode.
- The storage performance of Ni based cathode is superior to that of Co based cathode.
- Change of both cathode surface and bulk affects the storage performance.

ARTICLE INFO

Article history:
Received 1 May 2013
Received in revised form
17 August 2013
Accepted 20 August 2013
Available online 6 September 2013

Keywords:
Scanning transmission electron energy-loss spectroscopy
Deterioration
Storage performance
Cycle performance
Lithium nickel cobalt aluminum oxide
Lithium-ion batteries

ABSTRACT

Ni-based $LiNi_{(1-x-y)}Co_xAl_yO_2$ (NCA) and $LiCoO_2$ (LCO) cathode materials taken out of lithium-ion cells after storage for 2 years at 45 °C were analyzed by various spectroscopic techniques. X-ray photoelectron spectroscopy exhibited that there was no difference between NCA and LCO. On the other hand, scanning transmission electron microscopy–electron energy-loss spectroscopy demonstrated there was a remarkably large difference between the two cathode materials. Ni-$L_{2,3}$ energy-loss near-edge structure (ELNES) spectra of the NCA showed a peak at about 856.5 eV, which was assigned to trivalent nickel, was maintained even after storage, indicating that the NCA had no significant change in its surface structure during storage. On the other hand, in the Co-$L_{2,3}$ ELNES spectra of the LCO a peak at about 782.5 eV, which was assigned to trivalent cobalt, significantly shifted to the lower energies after storage. These results suggest that crystal structure change of the active material surface is a predominant reason of deterioration during the storage test.

1. Introduction

Lithium-ion batteries are widely used in portable devices such as notebook personal computers (PCs), cellular phones and digital still camera because they have high energy density. With a rise in awareness of environmental issues, lithium-ion batteries are expected to be applied to high-power applications and electric energy storage use. For EV and household electric energy storage applications, longer calendar life than conventional usage is required. Batteries are often charged to high states of charge (SOC), and used in wide ranges of SOC during charge/discharge cycles.

Ni-based oxides, $LiNi_{(1-x-y)}Co_xAl_yO_2$ (NCA), have been considered as one of the most promising cathode materials because of their high capacity and low cost. It has been reported that partial substitution of Ni by Co and Al improved both thermal stability and cyclability [1–3]. However, lithium-ion batteries with the NCA cathode material were remarkably degraded during charge/discharge cycling and storage at high temperatures. The US Department of Energy's Advanced Technology Development (ATD) program suggested that high-power lithium ion batteries (0.8–1.0 A h, 93 W h kg^{-1}) for hybrid electric vehicle applications demonstrated the increased rates of area-specific impedance (ASI)

* Corresponding author. Tel.: +81 88 699 9395; fax: +81 88 699 9046.
E-mail address: watanabe.sho-ichiro@jp.panasonic.com (S. Watanabe).

0378-7753/$ – see front matter © 2013 Elsevier B.V. All rights reserved.
http://dx.doi.org/10.1016/j.jpowsour.2013.08.079

Table 1
Cell materials, cell capacity and test conditions of cylindrical 18650 cells.

Test condition		NCR18650	CGR18650E
Cathode material		$LiNi_{0.8}Co_{0.15}Al_{0.05}O_2$	$LiCoO_2$
Anode material		Graphite	Graphite
Cell capacity		2.9 A h	2.6 A h
Cycle test	Charge	CCCV; charged at 0.3 C rate up to 4.2 V 50 mA-cutoff	CCCV; charged at 0.7 C rate up to 4.2 V 50 mA-cutoff
	Charge rest	20 min	20 min
	Discharge	1.0 C rate, 2.5 V-cutoff	1.0 C rate, 3.0 V-cutoff
	Discharge rest	20 min	20 min
	Temperature	45 °C	45 °C
Interval storage – cycle test	Charge	CCCV; charged at 0.3 C rate up to 4.2 V 50 mA-cutoff	CCCV; charged at 0.7 C rate up to 4.2 V 50 mA-cutoff
	Charge rest	24 h	24 h
	Discharge	1.0 C rate, 2.5 V-cutoff	1.0 C rate, 2.5 V-cutoff
	Discharge rest	20 min	20 min
	Temperature	45 °C	45 °C
Storage test	Storage temperature	45 °C	45 °C
	Charge before storage	CCCV; charged at 0.3 C rate up to 4.1 V 50 mA-cutoff	CCCV; charged at 0.7 C rate up to 4.1 V 50 mA-cutoff
	Charge for checking capacity	CCCV; charged at 0.3 C rate up to 4.2 V 50 mA-cutoff	CCCV; charged at 0.7 C rate up to 4.2 V 50 mA-cutoff
	Discharge for checking capacity	0.2 C rate, 2.5 V-cutoff	0.2 C rate, 3.0 V-cutoff
	Capacity checking period	90 days	90 days

and power fade was strongly affected by temperature and time [4]. The SAFT team reported that the storage characteristics of a cylindrical lithium-ion cell (85–145 W h kg^{-1}) were affected by SOC, which could be ascribed to an imperfect solid electrolyte interface (SEI) formed on the cathode [5]. The mechanism of degradation upon aging and charge/discharge cycles was clarified by electrochemical impedance analysis and several surface analyses. The AC-impedance studies with symmetrical cells demonstrated that the interfacial resistance at the cathode was a more predominant factor in a rise of impedance [6].

Various spectroscopic methods such as X-ray photoelectron spectroscopy (XPS), FT-IR, attenuated total reflection-Fourier transform IR spectroscopy (ATR-FTIR) and high resolution hard XPS are often used for characterizing the cathode surface. Ostrovskii et al. and Anderson et al. clarified in XPS analysis that a cathode surface film consisted of a mixture of polycarbonates, LiF, Li_xPF_y and $Li_xPF_yO_z$ compounds [7]. Song et al. found in ex-situ ATR-FTIR analysis that dicarbonyl anhydride and carbonyl ester (RCOOR′) were formed on the surface of the cathode which was charged to 4.2 V [8]. Shikano et al. found that Li_2CO_3, hydrocarbons, $ROCO_2Li$, polycarbonate-type compounds and LiF were detected at the cathode surface by XPS and high-resolution hard XPS, and the amount of carbonates was increased during charge/discharge cycling [9]. Recently, Saito et al. have reported that lithium carbonate was mainly detected by ATR-FTIR spectroscopy and its amount decreased with decreasing SOC [10]. On the other hand, Abraham et al. proposed that an-oxygen-deficient surface layer was formed on an $Li(Ni,Co)O_2$ cathode due to oxygen-transfer reactions with the electrolyte [11].

The other spectroscopic analyses were also introduced to analysis a surface layer formed during charge/discharge cycles. Using in-situ X-ray absorption fine structure (XAFS), in situ micro XAFS and surface sensitive conversion electron yield (CEY) mode X-ray absorption spectroscopy (XAS), Ukyo et al. found that the valence of Ni in $LiNi_{0.8}Co_{0.15}Al_{0.05}O_2$ was converted from Ni^{3+} to Ni^{4+} during charging, whereas that of Co was hardly changed. Inactive Ni^{2+} atoms existed on the surface and the average valence of Ni was increased by charge/discharge cycling and aging [12,13]. The electron energy loss spectroscopy (EELS) and high resolution TEM revealed the an Ni–O layer with a rock salt (NaCl)-type crystal structure existed on the surface of cathode particle, and the appearance of an electrochemically inactive surface layer

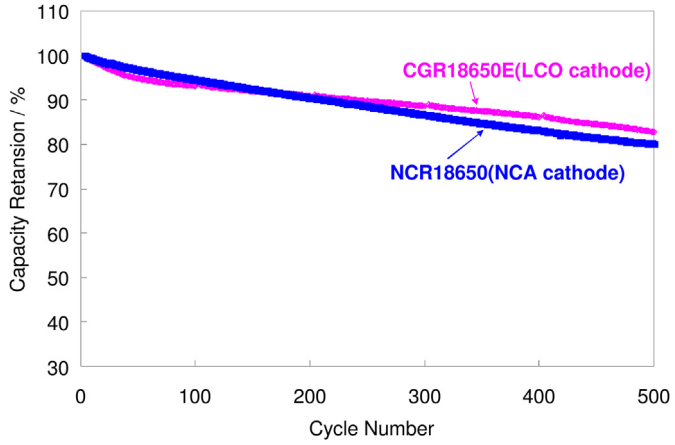

Fig. 1. Cycle performance of NCR18650 (NCA cathode) and CGR18650 (LCO cathode) at 45 °C.

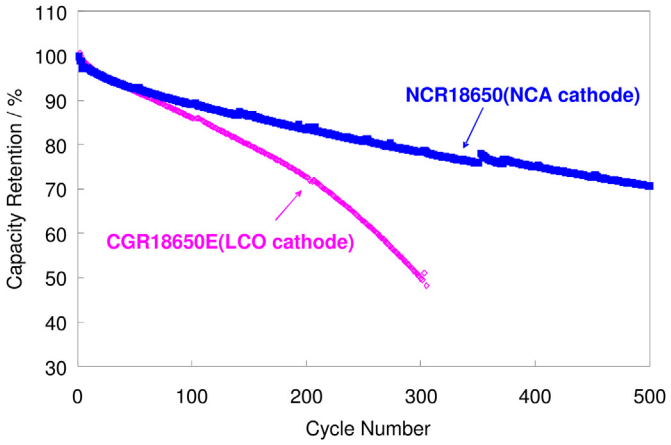

Fig. 2. Interval storage and cycle test performance of NCR18650 (NCA cathode) and CGR18650E (LCO cathode) at 45 °C.

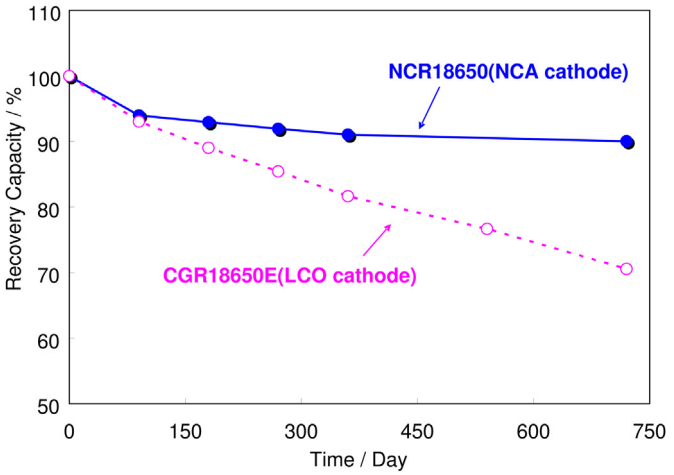

Fig. 3. Storage performance at 45 °C of NCR18650 (NCA cathode) and CGR18650 (LCO cathode) charged to 4.1 V.

contributed to the rise of cathode impedance during charge/discharge cycling and aging [15,16]. Tatsumi et al. proposed a schematic degradation model of $LiNi_{(1-x-y)}Co_xAl_yO_2$ with combining these spectroscopic methods [9,14].

Panasonic Co. launched the highest capacity and light weight lithium-ion battery series with the nickel-based NCA cathode in 2006. The energy density of a cylindrical 18650-type battery was 620 W h dm^{-3} and 230 W h kg^{-1} or more. Battery packs inside notebook PCs were used under severe conditions like full charge voltages and high temperatures of 40 °C or more because many customers used PCs with connecting the AC power supply. We noticed that the long term battery life of the NCA-cathode batteries (NCR18650) was several times as long as that of the LCO-cathode batteries (CGR18650E) [17]. The difference in long-term reliability between these two commercial lithium-ion batteries must be caused by the difference of cathode material. In this study, the change in anode and cathode surface in the two 18650-type cells was investigated by XPS, ICP and TEM-EELS during the interval storage and cycle tests imitating actual usage conditions by PC users in the market (discharge/charge and 24 h charge state storage at 45 °C), and normal cycle and storage tests and the capacity fade was determined by the reconstructed model cell method. Moreover, the mechanism of degradation was proposed on the basis of these results.

2. Experimental

2.1. Accelerated calendar and cycle life tests for cylindrical 18650 cells

Two cylindrical battery cells made by Panasonic Co. were used in this study. The NCA and LCO cathode cells are NCR18650 (2900 mA h) and CGR18650E (2600 mA h) whose cathode and anode materials, cell capacity and test conditions are shown in Table 1, respectively.

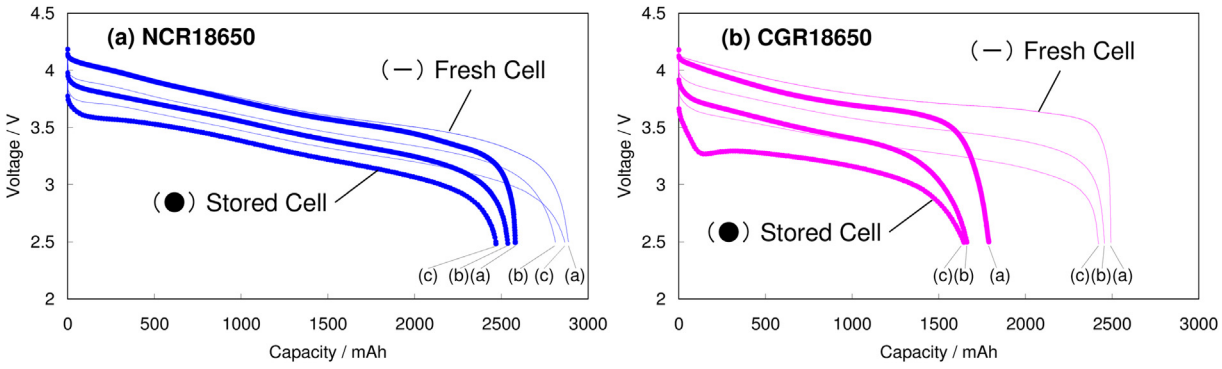

Fig. 4. Rate performances of the (a) NCR18650 and (b) CGR18650. The cells were charged up to 4.2 V by CVCC until the current reduced to 0.05 C and discharged at (a) 0.2 C, (b) 1 C and (c) 2 C rate at 25 °C. Straight line and closed circles indicate (−) fresh cell and (●) cell stored for 2 years at 45 °C after being charged to 4.1 V, respectively.

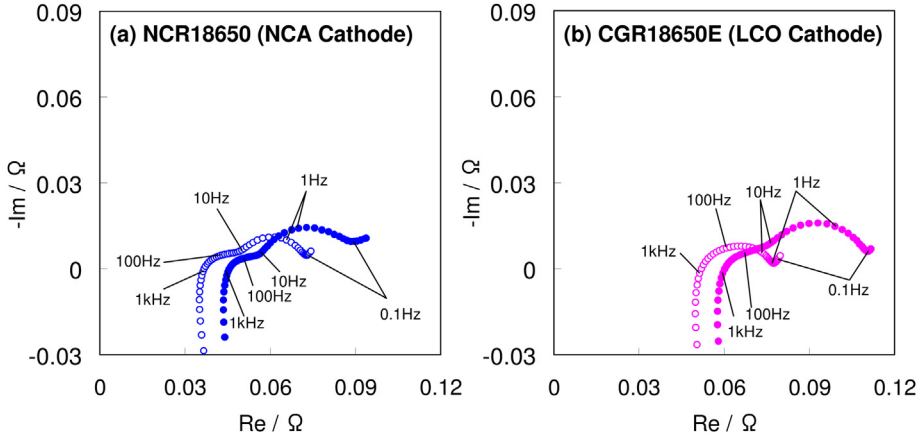

Fig. 5. Nyquist plots of (a) NCR18650 and (b) CGR18650E which were (○) fresh or (●) stored for 2 years at 45 °C after being charged to 4.1 V. Each impedance measurement was performed at 100% SOC and a temperature of 25 °C.

The nickel-based oxide cathode/graphite cell was composed of nickel-based oxide cathode, graphite anode, electrolyte and microporous polyethylene/heat-resisting polymer layer-coated separator. The nickel-based oxide cathode was composed of a mixture of $LiNi_{0.8}Co_{0.15}Al_{0.05}O_2$, carbon black and poly(vinylidene fluoride), and aluminum foil. The cobalt-based oxide cathode/graphite cell was the same as the nickel-based oxide cathode/graphite cell except for the cathode active material. Electrolyte was a mixture of ethylene carbonate (EC), ethylmethyl carbonate (EMC) and dimethyl carbonate (DMC) containing 1 mol L^{-1} (=M) lithium hexafluorophosphate ($LiPF_6$).

The cycle tests, the interval storage − cycle tests and the storage tests were performed according to protocols in Table 1. The protocols for the interval storage and cycle tests imagine user's usage in Note-type PC.

For cycle test of NCR18650 cell, the cell was charged at 870 mA (0.3 C rate) up to 4.2 V followed by constant voltage until the current reduced to 50 mA. The cell was then discharged to 2.5 V at 2900 mA (1 C rate). For cycle test of CGR18650 cell, the cell was charged at 1820 mA (0.7 C rate) up to 4.2 V followed by constant voltage until the current reduced to 50 mA. The cell was then discharged to 3.0 V at 2600 mA (1 C rate). Twenty minutes of relaxation were used after charging and discharging. For interval storage − cycle test, 24 h of relaxation was used after charging, and the other conditions were the same as cycle test. Before storage test of NCA18650 cell and CGR18650 cell, the cells were charged at 870 mA (0.3 C rate) and 1820 mA (0.7 C rate) until voltage reached 4.1 V at which constant-voltage charging was applied until current reduced to 50 mA. The charged cells were stored for 720 days together with capacity examined at 580 mA or 520 mA (0.2 C rate) every 90 days. When checking capacity during storage, the cells were charged to 4.2 V.

Cycle tests, interval storage-cycle tests and storage tests were done in a temperature of 45 °C.

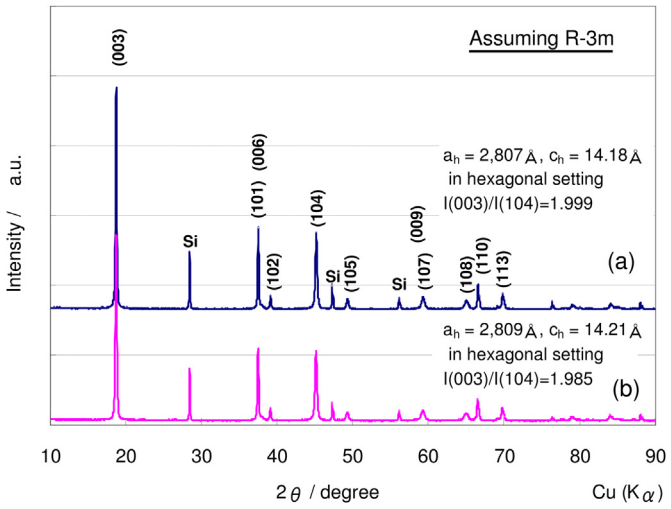

Fig. 7. X-ray diffraction patterns of NCA cathode taken out from the charged NCR18650; (a) fresh cathode material and (b) stored cathode material. Miller indexes and lattice parameters were given by assuming a hexagonal lattice. The lattice parameters were obtained by a least-squares method using nine diffraction lines depending on the number of well-defined diffraction lines. Storage condition; the cells were stored for 2 years at 45 °C after being charged to 4.1 V.

2.2. The model cell and impedance analysis

In order to determine which electrode was degraded, both the cathode and anode were taken out of each 18650 cell and used for assembling a 2016 coin cell with the lithium metal foil as a counter electrode under Ar atmosphere. An electrolyte and a separator of the coin cell were the same as those of the 18650 cell. Impedance measurements were performed using a Solartron 1260/1286

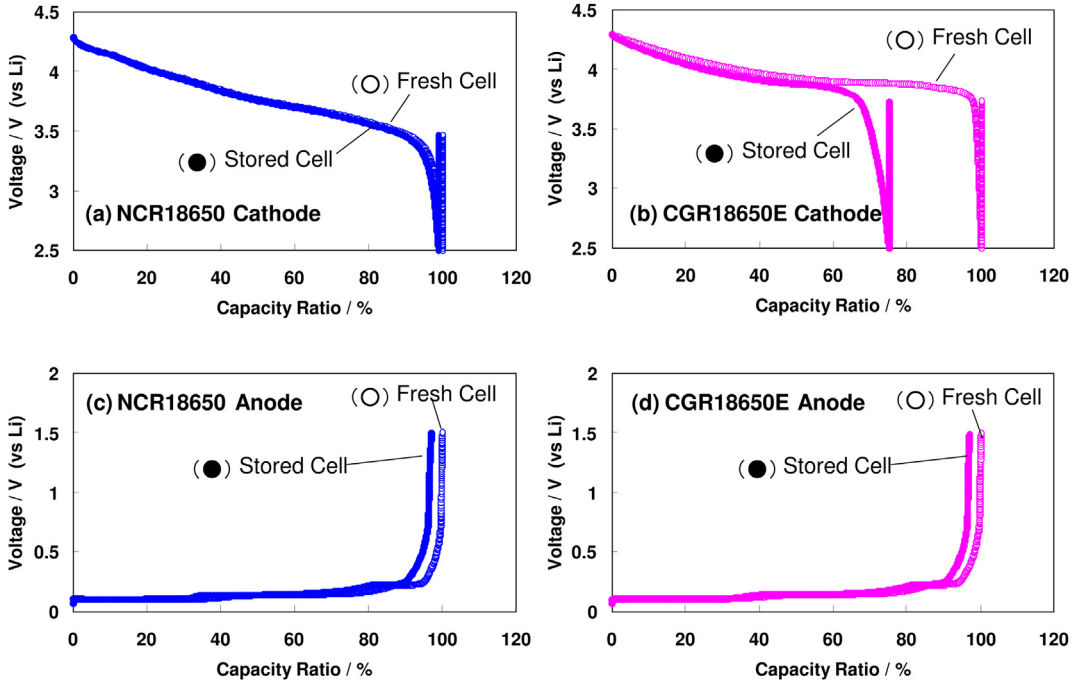

Fig. 6. Discharge curves of (a) NCA cathode of NCR18650, (b) LCO cathode of CGR18650E, (c) graphite anode of NCR18650, (d) graphite anode of CGR18650E; the data of cathode obtained from the (○) fresh cell and (●) cell stored for 2 years at 45 °C after being charged to 4.1 V, respectively. Percentage of the initial value of discharge capacity was shown. Storage condition; the cells were stored for 2 years at 45 °C after being charged to 4.1 V.

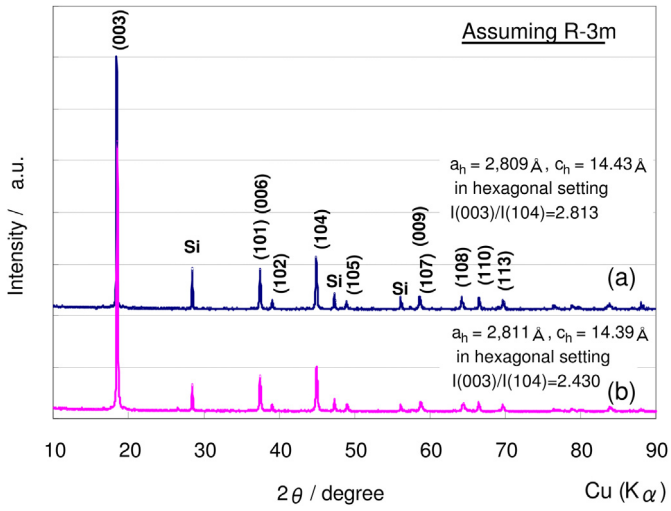

Fig. 8. X-ray diffraction patterns of LCO cathode taken out of the charged CGR18650E; (a) fresh cathode material and (b) stored cathode material. Miller indexes and lattice parameters were given by assuming a hexagonal lattice. The lattice parameters were obtained by a least-squares method using nine diffraction lines depending on the number of well-defined diffraction lines. Storage condition; the cells were stored for 2 years at 45 °C after being charged to 4.1 V.

frequency response analyzer system. The amplitude of the ac signal was 10 mV over the frequency range between 1 MHz and 1 mHz in this study. All measurements were carried out at 25 °C. The capacity fade and impedance change of the cathode and anode were compared with their initial conditions.

2.3. Surface and bulk analysis

XRD patterns were collected with a Panalytical X'Celerator detector equipped with a Cu target X-ray tube and a diffracted beam monochromator. Each XRD measurement was performed every 0.05° over a scattering angle range between $2\theta = 10°$ and 90° and the counting time was 10 s. SEM images were obtained with a Hitachi S-4500 scanning electron microscope equipped with an energy-dispersive X-ray (EDX) analyzer.

Surface structure of each cathode material was characterized by XPS and scanning transmission electron microscopy (STEM)-selected area electron diffraction (SAED)/EELS. XPS analysis was performed with a Perkin–Elmer PHI 560/ESCA-SAM system. XPS spectra were obtained after several times of Ar^+-sputtering with 4 keV energy ions and a current beam of 0.36 μA cm^{-2}. A sample for the XPS analysis was excited with 1486.6 eV energy Al Kα X-rays. Inductively coupled plasma atomic emission spectrometry (ICP-AES) measurement was performed using ICPS-7500 in order to quantify the amount of metal deposited on the anode surface. STEM-SAED/EELS analysis was conducted with a 200 kV JEOL JEM-2100F equipped with a parallel electron energy loss spectrometer (Gatan 863). XRD and SEM were used to study the phase change and microscopic morphology for each active material after storage. For surface and bulk analyses, each cell was charged to a voltage of 4.1 V at 0.2 C rate and then the voltage was kept until the current was reduced to 0.05 C rate. After charging, the cell was disassembled. The samples taken out of the disassembled cells were washed with dry DMC and evaporated at room temperature.

3. Results and discussion

3.1. Performance of 18650 cells

Fig. 1 shows cycle performance for an NCR18650 (NCA cathode) and a CGR18650E (LCO cathode) at 45 °C. This figure indicates there are only a few differences in cycle performance between both cells. However, as for the interval storage and cycle test performance, the NCR18650 was much superior to the CGR18650E as shown in Fig. 2.

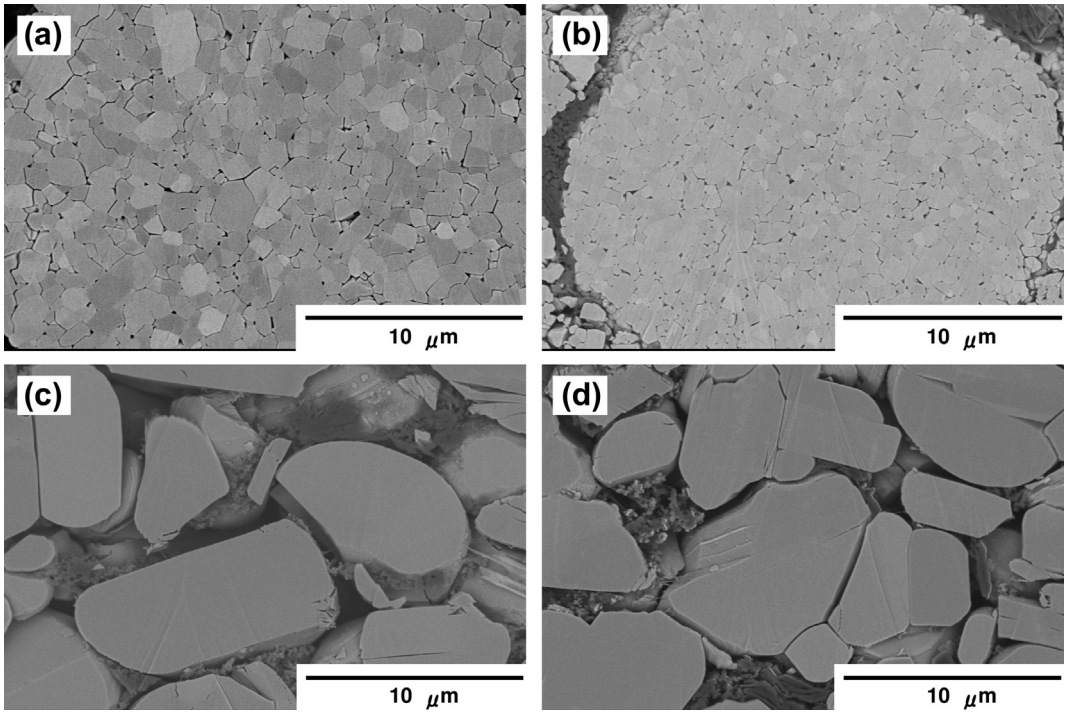

Fig. 9. SEM images of cathode material particles; (a) fresh NCR18650 cathode, (b) stored NCR18650 cathode, (c) fresh CGR18650 cathode and (d) stored CGR18650 cathode. Storage condition; the cells were stored for 2 years at 45 °C after being charged to 4.1 V.

The life time of the 70% capacity retention for the NCR18650 was twice longer than that for the CGR18650E.

In order to verify the difference, the capacity fade analysis during a long term storage test was performed. Fig. 3 shows storage performance at 45 °C for the NCR18650 and CGR18650E after they were charged to 4.1 V. The NCR18650 showed better storage performance than the CGR18650E. The NCR18650 maintained about 90% of the initial capacity even after storage for 2 years at 45 °C.

Fig. 4 shows rate performance for the NCR18650 and CGR18650E which were fresh or stored for 2 years at 45 °C after being charged to 4.1 V. As be seen from Fig. 4, the capacity fade and polarization of the CGR18650E was remarkably increased during the storage for 2 years.

Fig. 5 shows ac impedance spectra of the NCR18650 and CGR18650E which were fresh or stored for 2 years at 45 °C after being charged to 4.1 V. Each impedance measurement was performed at 100% SOC and a temperature of 25 °C. The charge transfer resistance (R_{ct}) was evaluated from the lower frequency semicircle in each Nyquist plot. The R_{ct} values for the fresh and stored NCR18650 were 0.0262 and 0.0356 Ω, respectively, while those for the fresh and stored CGR18650E were 0.0231 and 0.0407 Ω, respectively. The impedance of both cells was increased during storage, but its increment for the CGR18650E was much larger than that for the NCR18650.

3.2. Analysis of disassembled battery

To reassemble a 2016 coin cell, the cathode or anode active materials taken out of the fresh and stored cells were used with a lithium metal counter electrode.

Fig. 6 shows discharge curves of each reassembled coin cell operated in the voltage range of 2.5–4.3 V or 0.01–1.5 V at a constant current of 0.1 C at 25 °C. As be seen from Fig. 6(a) and (b), in the discharge process no significant capacity fade was observed for

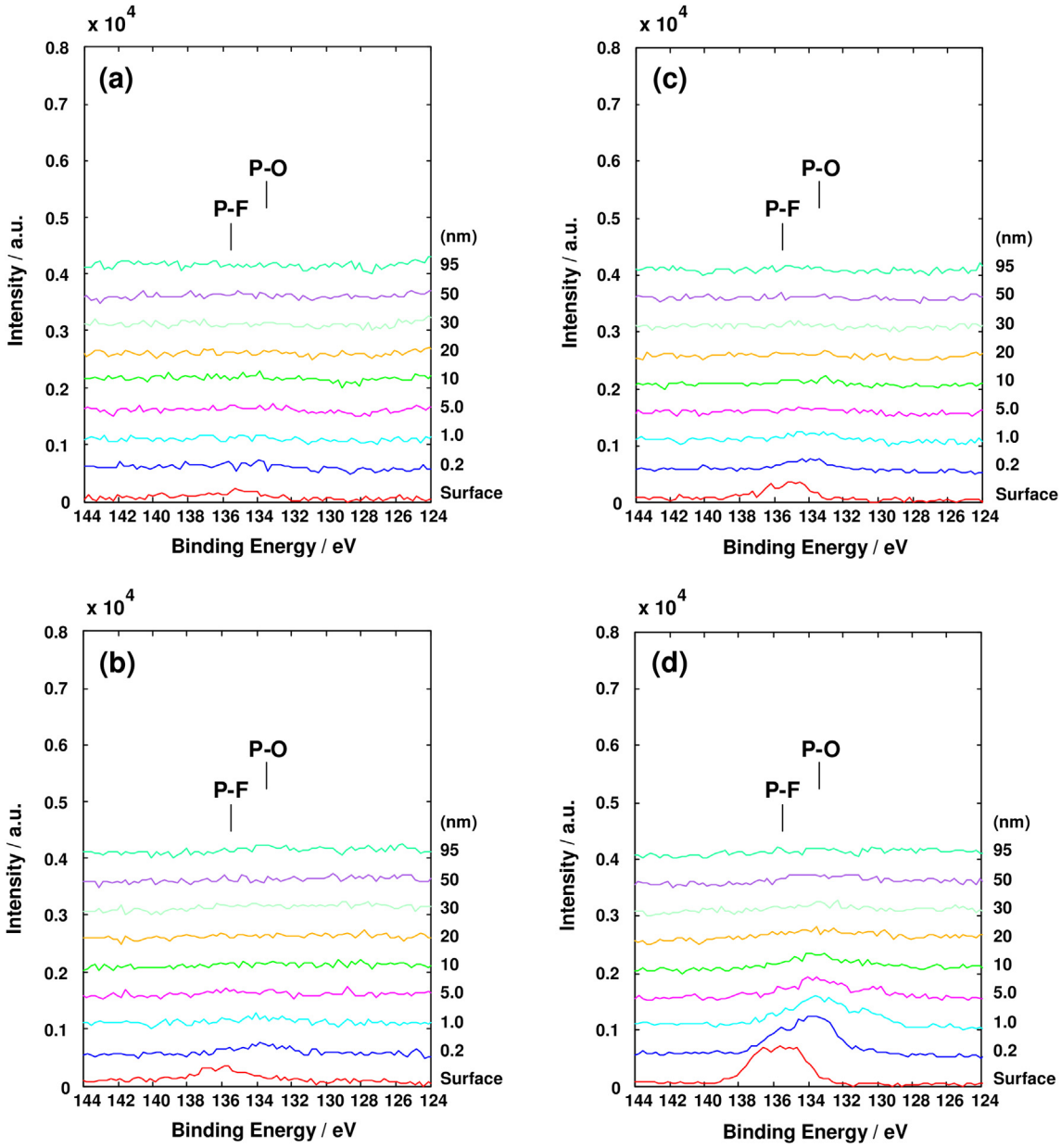

Fig. 10. P2p core level XPS spectra for cathode surface; (a) fresh NCA cathode, (b) fresh LCO cathode, (c) stored NCA cathode and (d) stored LCO cathode. Storage condition; the cells were stored for 2 years at 45 °C after being charged to 4.1 V.

the NCA cathode after storage, while 30% capacity fade was observed for the LCO cathode after storage. Moreover, as shown in Fig. 6(c) and (d), in the charge process the notable capacity fade was not observed for the graphite anode in both NCR18650 and CGR18650E. These results suggest that the difference in capacity fade of lithium ion cells during high temperature storage shown in Figs. 2 and 3 is ascribed to the degradation of cathode.

ICP analysis confirmed that the lithium composition of both cathode active materials, NCA and LCO, before and after the storage tests were equal when each cell was charged to a voltage of 4.1 V before every analysis below.

Figs. 7 and 8 show XRD patterns of the fresh and stored NCA and LCO cathode active materials, respectively. The samples for XRD were prepared by clipping from 4.1 V charged cathode and then mixing with the standard reference material (NIST 640c Si). All diffraction lines for fresh and stored cathode active materials were indexed by assuming a hexagonal lattice. All XRD patterns of the fresh and stored NCA and LCO cathode active materials were identical as α-$NaFeO_2$ having a space group of R-3m. Ramadass et al. pointed out that peak intensities of (003), (006), and (104) planes for the LCO changed during the cycle tests at high temperatures [18]. However, as can be seen from Figs. 7 and 8, additional diffraction lines and line broadening of each diffraction line were not specifically observed, indicating that the core structure of the cathode materials was not damaged during 2 year storage at 45 °C. The integrated intensity ratio of (003) to (104) lines in each XRD pattern indicates the amount of cobalt or nickel ion mixing into Li layer (cation mixing). There was no significant difference in the intensity ratio between fresh and stored NCA cathode active materials. On the other hand, the intensity ratio between fresh and stored LCO cathode active materials showed a significant change.

SEM images of cathode active materials taken out of the disassembled cells are shown in Fig. 9. No notable difference in cathode particles morphology between the fresh and stored

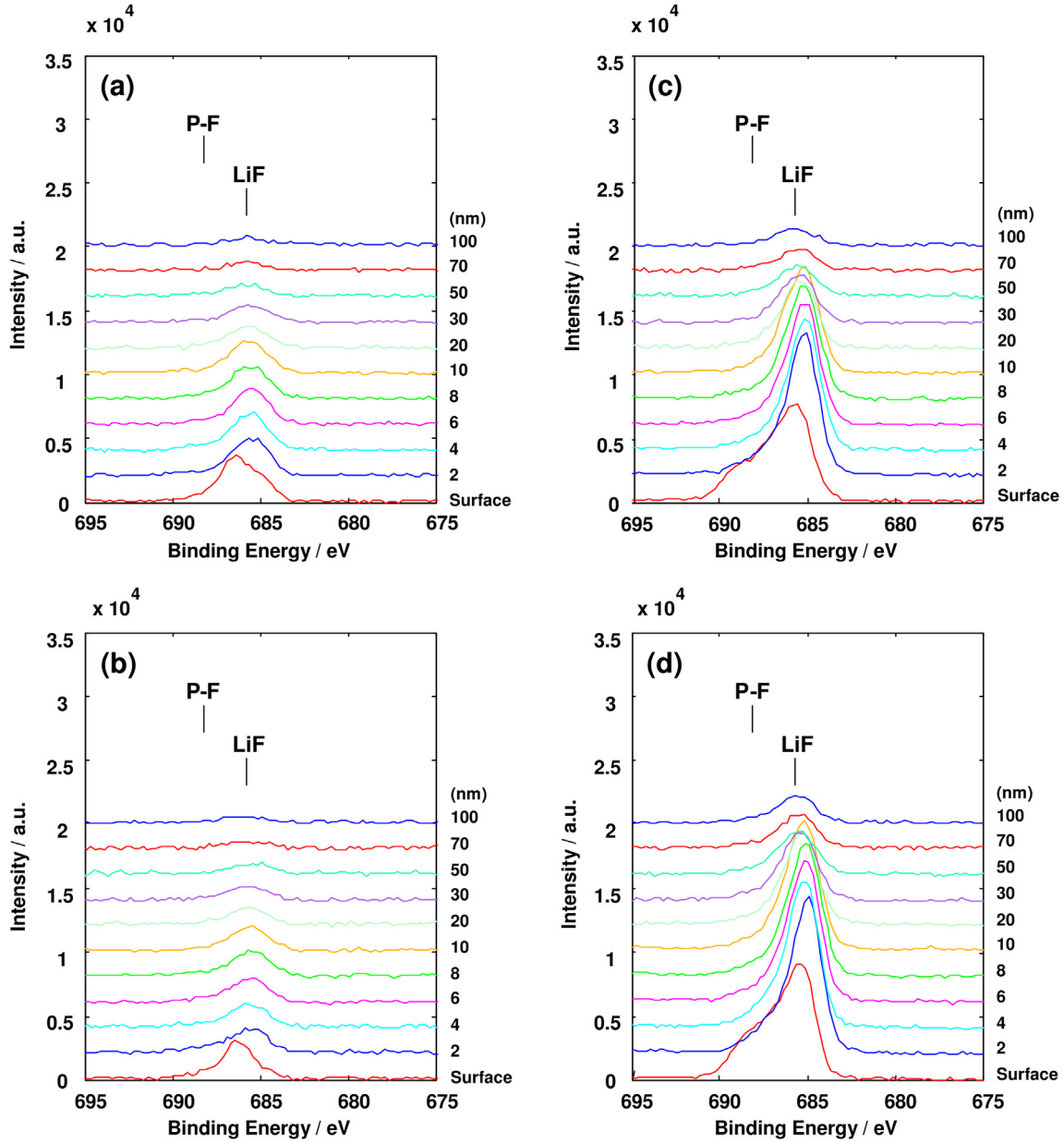

Fig. 11. F1s core level XPS spectra for anode surface (a) fresh anode of NCR18650, (b) fresh anode of CGR18650, (c) stored anode of NCR18650 and (d) stored anode of CGR18650. Storage condition; the cells were stored for 2 years at 45 °C after being charged to 4.1 V.

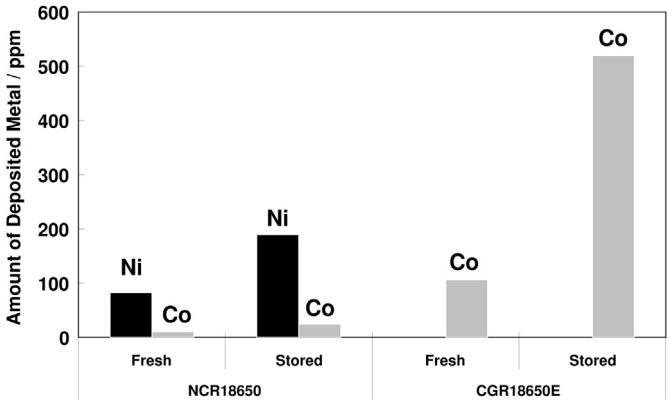

Fig. 12. Amount of metal deposition on the anode surface of fresh cell and cell stored for 2 years at 45 °C; deposited (■) Ni and (■) Co.

samples was observed. In addition, we analyzed the electrolyte composition and separator SEM morphology and separator Gurley number change after storage, but the substantial change was not recognized.

These results show that the difference in degradation of LCO cathode and NCA cathode at high temperature long term storage is due to ease of forming cation mixing.

Besides, the influence of cathode surface for battery degradation as has been previously pointed out [19] is discussed below.

3.3. Analysis of electrode/electrolyte interface

In order to obtain more information on the cathode/electrolyte interface, the surface of the NCA and LCO cathodes was analyzed by XPS. Fig. 10 shows P2p core level spectra for the NCA and LCO cathodes before and after 2 years storage at 45 °C. P2p core level was used because of eliminating inappropriate influence of PVdF as a cathode binder. In the P2p core level spectra, peaks at 135.5 and 133.5 eV are assigned to a P–F bond and a P–O bond, respectively. Anderson et al. clarified these two peaks were ascribed to Li_xPF_y and $Li_xPF_yO_z$ compounds which were formed on the cathode surface [20]. The thickness of the surface layer for the NCA cathode scarcely increased during the long-term storage, while that for the LCO cathode increased by only several nanometers. So the formation of surface layer does not seem to be a predominant factor for the deterioration of cathode performance.

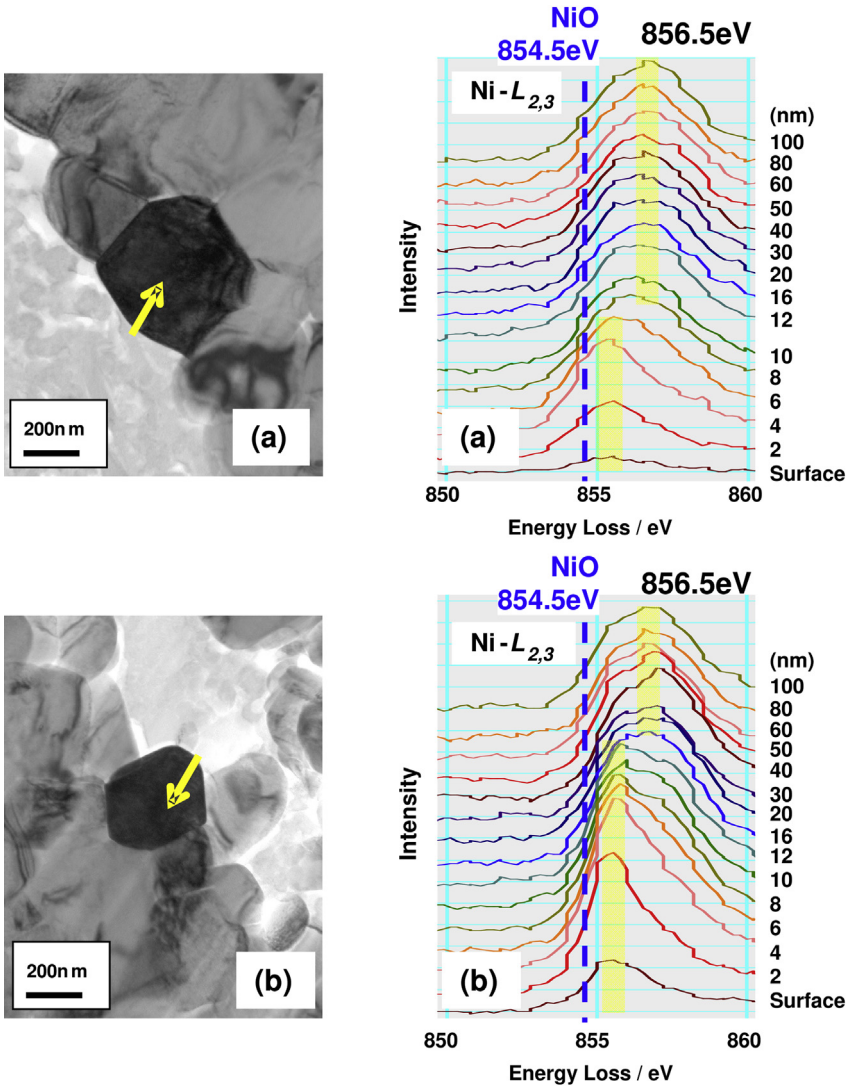

Fig. 13. Cross section TEM images and Ni-$L_{2,3}$ ELNES spectra from NCA cathode material taken out from the charged NCR18650; (a) fresh cathode material and (b) stored cathode material. Dash lines show the peak positions of Ni-$L_{2,3}$ ELNES spectrum from the surface of NiO particle. Storage condition; the cells were stored for 2 years at 45 °C after being charged to 4.1 V.

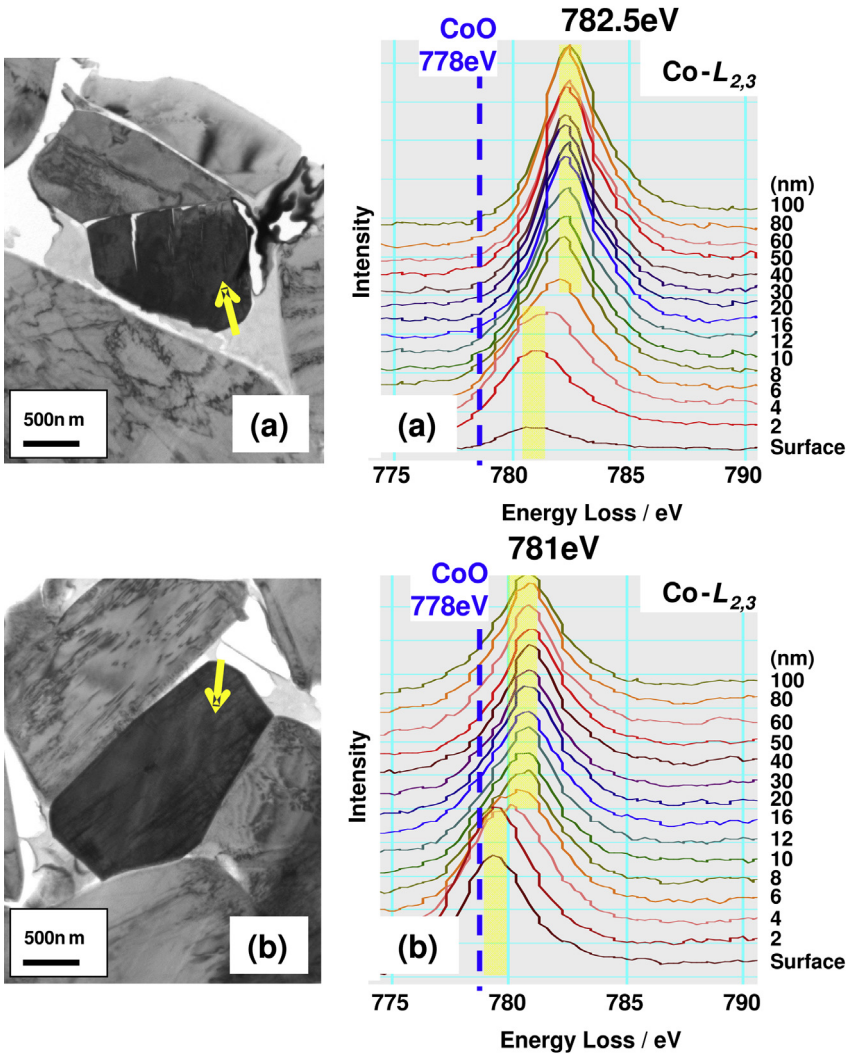

Fig. 14. Cross section TEM images and Co-$L_{2,3}$ ELNES spectra from the LCO cathode material taken out from the charged CGR18650E; (a) fresh cathode material and (b) stored cathode material. Dash lines show the peak positions of Co-$L_{2,3}$ ELNES spectrum from the surface of CoO particle. Storage condition; the cells were stored for 2 years at 45 °C after being charged to 4.1 V.

Fig. 11 shows F1s core level spectra for the anode surface of NCR18650 and CGR18650E before and after 2 years storage at 45 °C. In the F1s core level spectra, peaks at 688 and 686 eV are assigned to P—F and Li—F, respectively. In each spectrum these two peaks were observed, suggesting the formation of the anode surface layer or SEI with LiF and hydrolysis products such as $LiPOF_3$ and $Li_xPO_yF_z$ compounds. $LiPF_6$ as an electrolyte often decomposes to PF_5 and LiF, and PF_5 readily reacts with trace amount of moisture to form HF as a

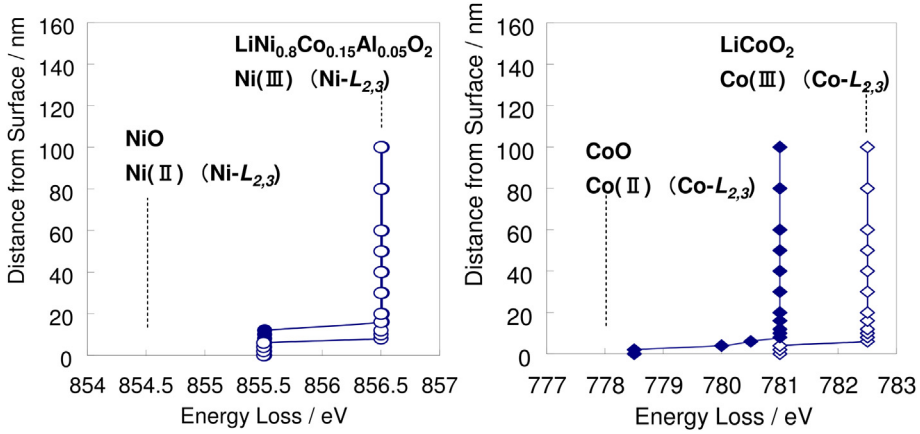

Fig. 15. The Ni- and Co-$L_{2,3}$ ELNES peak position changes from surface of charged cathode particle; (○) Ni-$L_{2,3}$ of NCA before storage, (●) Ni-$L_{2,3}$ of NCA after storage, (◇) Co-$L_{2,3}$ of LCO before storage, (◆) Co-$L_{2,3}$ of LCO after storage. Storage condition; the cells were stored for 2 years at 45 °C after being charged to 4.1 V.

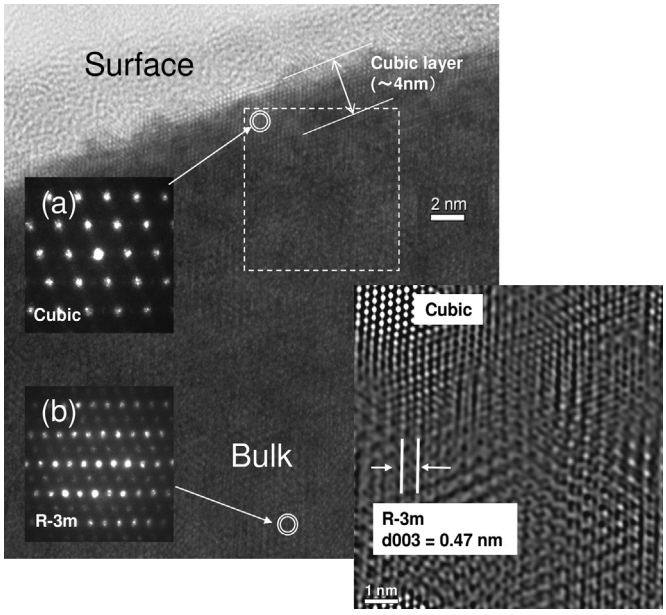

Fig. 16. The high resolution image and convergent beam electron diffraction patterns of NCA cathode material taken out from stored NCR18650. Storage condition; the cells were stored for 2 years at 45 °C after being charged to 4.1 V.

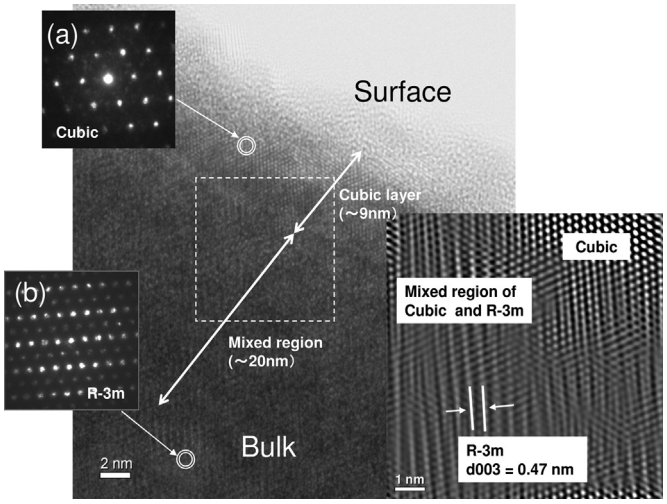

Fig. 18. The high resolution image and convergent beam electron diffraction patterns of LCO cathode material taken out from stored CGR18650E. Storage condition; the cells were stored for 2 years at 45 °C after being charged to 4.1 V.

hydrolysis product. Consequently, HF reacts with Li-carbonate compounds to form LiF [21]. The anode surface layer after the long-term storage for the NCR18650 had thickness close to that for the CGR18650E strongly suggesting that the formation of SEI on the anode surface also did not seem to be a predominant factor for the deterioration of cathode performance.

Fig. 12 shows the amount of Ni and Co components in deposits on the anode surface of NCR18650 and CGR18650E before and after 2 years storage at 45 °C. The amount of the Ni and Co components was quantified by ICP-AES. Fig. 12 clearly indicated that in both cases Co and Ni dissolved from the cathode were deposited on the graphite anode surface. Amatucci et al. reported that there was a linear correlation between the capacity loss of the $LiCoO_2$ cathode during high voltage cycling tests and the amount of Co deposited on the anode [22]. In the present study, the amount of Ni dissolved from the NCA cathode during the long-term storage was less than half that of Co dissolved from the LCO cathode. This implies that the amount of Co and Ni dissolved from cathode material can be related to the change in surface crystal and electronic structures of the nickel-based and the cobalt-based oxide cathodes.

STEM-EELS was used in order to investigate the changes in the local structure and the electronic structure of active material before and after storage at 45 °C for 2 years. Figs. 13 and 14 show the Ni-$L_{2,3}$ energy-loss and the Co-$L_{2,3}$ energy-loss near-edge structure (ELNES) spectra for the NCA and LCO cathode materials in the 18650 cells before and after storage at 45 °C for 2 years. Fig. 15 summarized the Ni- and Co-$L_{2,3}$ ELNES peak depth profiles of cathode particle before and after storage.

The Ni-$L_{2,3}$ ELNES spectra were acquired in a depth range from the surface to 100 nm for a selected NCA cathode material particle. The NiO powder as the standard has a peak at 854.5 eV, indicating that it is assigned to divalent nickel. In contrast, the peak at 856.5 eV is assigned to trivalent nickel. The Ni-$L_{2,3}$ ELNES spectra after storage exhibited that the peak at 856.5 eV in a depth range of 6–10 nm was shifted to 855.5 eV during the storage test, suggesting that the surface layer composed of oxygen deficient NiO became thick. It was reported that the Ni^{4+} ions which existed in the charged state could be transformed into Ni^{2+} with the oxidation of the electrolyte and solvents at the cathode/electrolyte interface, and the structure change into rock-salt type and oxygen loss also occurred simultaneously [23]. In this study, the charged NCA oxidized the electrolyte with oxygen loss to form the nano-order surface layer of lithium/oxygen-deficient $Li(Ni,Co)O_2$ with the rock-salt structure at the cathode/electrolyte interface as follows [11]:

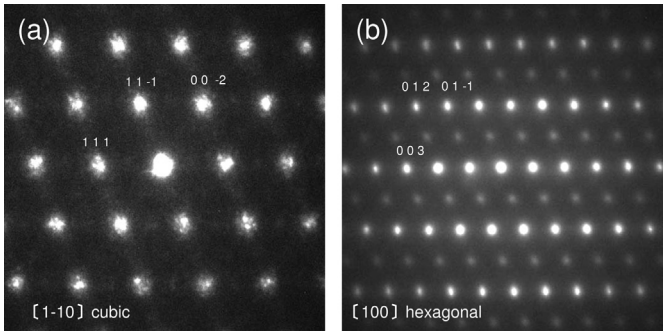

Fig. 17. Experimental electron diffraction patterns exhibiting only fundamental reflections collected from stored NCA cathode material taken out from the charged NCR18650, (a) surface area which is indexed to the (1–10) zone axis ((111) $d = 0.24$ nm), (b) bulk area which is indexed to the (100) zone axis ((003) $d = 0.47$ nm).

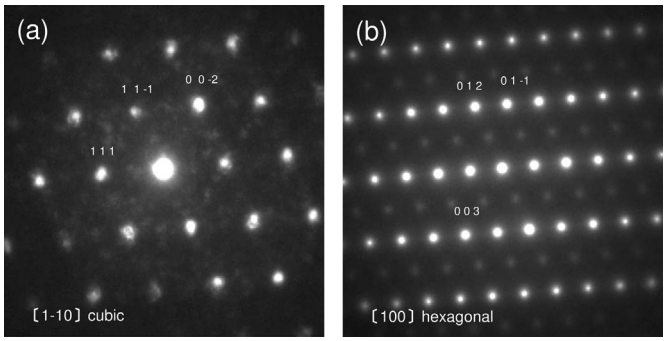

Fig. 19. Experimental electron diffraction patterns exhibiting only fundamental reflections collected from stored LCO cathode material taken out from the charged NCGR18650E, (a) surface area which is indexed to the (1–10) zone axis ((111) $d = 0.24$ nm), (b) bulk area which is indexed to the (100) zone axis ((003) $d = 0.47$ nm).

$$Li_{1-a}(Ni,Co)^{3+/4+}O_2(\text{delithiation state}) \rightarrow Li_{1-a}(Ni,Co)^{3+/2+}O_{2-\delta}(\text{oxygen loss})(0 < a < 1,\ 0 < \delta) \quad (1)$$

The Co-$L_{2,3}$ ELNES spectra for the LCO cathode material in the CGR18650E before and after storage are shown in Fig. 14. The peak positions of CoO powder for the standard of divalent cobalt are shown in Figs. 14 and 15. Before storage the peak at 782.5 eV assigned to trivalent cobalt was observed underneath the surface layer with thickness of around 10 nm, but after storage it shifted to 781 eV as shown in Fig. 15. The crystal structure of the surface layer can be identified as a CoO-like rock-salt structure by selected area electron diffraction (SAED) analysis, as discussed by some groups [13,19].

Figs. 16–19 show high resolution TEM images and experimental electron diffraction patterns for surface and bulk of active materials after storage at 45 °C for 2 years. Figs. 16 and 17 show the image of stored NCA bulk-surface with two micro diffraction patterns layer. Figs. 16 and 18 exhibited that the surface layer of NCA and LCO had about several nanometers in thickness and a cubic rock salt-type NiO and CoO structures. In the case of stored LCO particle, three types of micro diffraction layers were observed in Fig. 18. The thickness of the surface cubic rock-salt layer was about 9 nm which was thicker than that of the NCA particle. Moreover, a mixed layer which was composed of the α-$NaFeO_2$-type *R*-3*m* and cubic rock-salt structures was formed underneath the LCO surface layer, and its thickness was about 20 nm. The lithium nickel/cobalt oxide layer with rock-salt structure formed on the NCA/LCO surface can bring low lithium ion conductivity and low electric conductivity, which caused an increase in cathode impedance. The growth of the rock-salt type surface layer for LCO was much faster than that for NCA. The difference of growth rate of the rock-salt type surface layer may be due to the difference in amount of Ni and Co dissolution shown in Fig. 12. This is responsible for a big difference in storage characteristics between LCO and NCA.

4. Conclusion

In order to verify good long life reliability of NCR18650 (NCA cathode), its capacity fade analysis during the long-term storage test was investigated and compared with CGR18650E (LCO cathode). The findings obtained in this study are summarized as follows,

(1) NCR18650 was greatly superior to CGR18650E in the storage characteristics.
(2) The increase in impedance and capacity fade was mainly attributed to the degradation of the cathode, and the deterioration of LCO cathode was larger than that of NCA cathode.
(3) SEI on NCA and LCO cathode surface analyzed by XPS was composed of almost same elements and had same thickness level, suggesting that SEI was not the main factor of the difference in degradation behavior between NCA and LCO cathodes.
(4) Change in the surface crystal/electronic structures and the cation mixing of NCA cathode material during the long-term storage at high temperature was much smaller than that of LCO cathode material, indicating that NCA had excellent storage characteristics.

In this paper, the difference between the degradation of LCO/graphite cell and that of NCA/graphite cell was particularly discussed. The results of detailed analysis on the influence of cycling for degradation of the performance of these cells will be discussed in next paper.

Acknowledgments

This work was supported by the “LEAD” program of the New Energy and Industrial Technology Development Organization (NEDO). The authors express their thanks to members of Lithium ion Battery Business Unit (A. Nagasaki, N. Yamamoto and H. Kaiya) and Prof. Hiroshi Inoue in Osaka Prefecture University.

References

[1] T. Ohzuku, A. Ueda, M. Kouguchi, J. Electrochem. Soc. 142 (1995) 4033.
[2] H. Arai, M. Tsuda, Y. Sakurai, J. Power Sources 90 (2000) 76.
[3] A. Kinoshita, K. Yanagida, A. Yanai, Y. Kida, A. Funahashi, T. Nohma, I. Yonezu, J. Power Sources 102 (2001) 283.
[4] I. Bloom, S.A. Jones, V.S. Battaglia, G.L. Henriksen, J.P. Christophersen, R.B. Wright, C.D. Ho, J.R. Belt, C.G. Motloch, J. Power Sources 124 (2003) 538.
[5] M. Broussely, Ph. Biensan, F. Bonhomme, Ph. Blanchard, S. Herreyre, K. Nechev, R.J. Staniewicz, J. Power Sources 146 (2005) 90.
[6] C.H. Chen, J. Liu, M.E. Stoll, G. Henriksen, D.R. Vissers, K. Amine, J. Power Sources 128 (2004) 278.
[7] A.M. Andersson, D.P. Abraham, R. Haasch, S. MacLaren, J. Liu, K. Amine, J. Electrochem. Soc. 149 (2002) A1358.
[8] S.W. Song, G.V. Zhuang, P.N. Ross Jr., J. Electrochem. Soc. 151 (2004) A1162.
[9] M. Shikano, H. Kobayashi, S. Koike, H. Sakaebe, E. Ikenaga, K. Kobayashi, K. Tatsumi, J. Power Sources 174 (2007) 795.
[10] Y. Saito, M. Shikano, H. Kobayashi, J. Power Sources 196 (2011) 6889.
[11] D.P. Abraham, R.D. Twesten, M. Balasubramanian, I. Petrov, J. McBreen, K. Amine, Electrochem. Commun. 4 (2002) 620.
[12] T. Nonaka, C. Okuda, Y. Seno, K. Koumoto, Y. Ukyo, Ceram. Int. 34 (2008) 859.
[13] T. Sasaki, T. Nonaka, H. Oka, C. Okuda, Y. Itou, Y. Kondo, Y. Takeuchi, Y. Ukyo, K. Tatsumi, S. Muto, J. Electrochem. Soc. 156 (2009) A289.
[14] H. Kobayashi, M. Shikano, S. Koike, H. Sakaebe, K. Tatsumi, J. Power Sources 174 (2007) 380.
[15] D. Mori, H. Kobayashi, M. Shikano, H. Nitani, H. Kageyama, S. Koike, H. Sakaebe, K. Tatsumi, J. Power Sources 189 (2009) 676.
[16] S. Muto, Y. Sasano, K. Tatsumi, T. Sasaki, K. Horibuchi, Y. Takeuchi, Y. Ukyo, J. Electrochem. Soc. 156 (2009) A371.
[17] S. Watanabe, M. Kinoshita, K. Nakura, in: Abstract of the IMLB Meeting, Montreal, 2010, Abstract.
[18] P. Ramadass, B. Haran, R. White, B.N. Popov, J. Power Sources 112 (2002) 614.
[19] D.P. Abraham, J. Liu, C.H. Chen, Y.E. Hyung, M. Stoll, N. Elsen, S. MacLaren, R. Twesten, R. Haasch, E. Sammann, I. Petrov, K. Amine, J. Power Sources 119 (2003) 511.
[20] D. Ostrovskii, F. Ronci, B. Scrosati, P. Jacobsson, J. Power Sources 94 (2001) 183.
[21] A.M. Andersson, M. Herstedt, A.G. Bishop, K. Edstrom, Electrochim. Acta 47 (2002) 1885.
[22] G.G. Amatucci, J.M. Tarascon, L.C. Klein, Solid State Ionics 83 (1996) 167.
[23] J. Vetter, P. Novak, M.R. Wagner, C. Veit, K.-C. Moller, J.O. Besenhard, M. Winter, M. Wohlfahrt-Mehrens, C. Vogler, A. Hammouche, J. Power Sources 147 (2005) 269.